Analyst

ROYAL SOCIETY OF CHEMISTRY

PAPER

View Article Online
View Journal | View Issue

Cite this: *Analyst*, 2022, **147**, 1589

Selection of healthy sperm based on positive rheotaxis using a microfluidic device†

Sandhya Sharma,[a,b] Md. Alamgir Kabir [a,b] and Waseem Asghar [*a,b,c]

For conception, sperm cells travel towards the oocyte. This journey is accomplished by only a few sperm cells, following various guidance mechanisms. Of these mechanisms, rheotaxis plays a significant role in guiding the sperm over a long distance. By taking advantage of this natural rheotaxis behavior of sperm, we have developed a microfluidic chip that isolates healthy sperm cells. The developed chip consists of different chambers separated by microchannels that facilitate separation of motile sperm cells from unprocessed semen samples with the help of fluid flow. The sperm cells are subjected to different velocities in different parts of the chip that direct functional sperm towards the collection chamber utilizing positive rheotaxis. The results from the developed microfluidic chip (with 0.5 μL min^{-1} flow rate) have shown almost 100% motility, a significantly higher percentage of morphologically normal sperm cells with lesser sperm DNA fragmentation than the control (no-flow) and raw semen sample. This chip satisfies the need of a clinical setting as it is low-cost, easy to operate and uses a small semen volume for sperm sorting.

Received 22nd December 2021,
Accepted 7th March 2022

DOI: 10.1039/d1an02311j

rsc.li/analyst

Introduction

The female genital tract is a highly selective environment that undergoes several physiological changes during the fertile window to facilitate fertilization.[1,2] These changes include optimal pH, decrease in the antimicrobial activity of leukocytes, and changes in the cervical mucus.[2] However, only a few hundred sperm cells reach the fallopian tubes, guided by specific mechanisms.[3] There are two mechanisms that have been widely regarded as the primary means of guiding sperm: chemotaxis[4,5] and thermotaxis.[6,7] However, chemotaxis is interrupted by fluid flow and distance while thermotaxis does not come into play until sperm cells are close to the temperature gradient generated by the oocyte.[8,9] By contrast, studies have demonstrated that rheotaxis is a significant factor that guides the sperm cells over a long distance during ovulation.[4,10] Rheotaxis is a mechanism wherein the sperm cells swim against the cervical mucus flow to reach the oocyte for fertilization.[1,10–12]

Multiple factors influence conception globally, however, 30–50% of these cases are caused by male infertility.[13] Assisted reproductive technologies (ART), which include *in vitro* fertilization (IVF), intrauterine insemination (IUI), and intracytoplasmic sperm injection (ICSI), have enabled infertile couples to achieve conception. To overcome infertility challenges in males, IUI, IVF, and ICSI have been practiced clinically; however, these technologies require healthy sperm cells for a successful ART outcome.[14] The success rate of IVF is only 25–30%.[15,16] The main reason behind the low success rate remains unclear, however, sperm defects are likely to be correlated with the IVF outcomes.[17] Studies have shown that the pregnancy rate is related to the motile and normal morphology of sperm cells.[18–20] Defects in sperm cells can reduce the binding affinity to the zona pellucida, failing to fertilize the oocyte.[21,22] For fertilization in the ICSI procedure, motile and morphologically normal sperm cells are clinically selected and injected into the oocyte.[23–25] Since motile and morphologically normal sperm cells hold biological significance, an optimal isolation method is essential.

Conventional methods of sperm sorting include the swim-up method, density gradient centrifugation, and sperm washing.[26,27] These methods involve multiple centrifugation steps that damage sperm morphology, induce significant DNA fragmentation and ROS in the healthy sperm cells.[28] Microfluidic platforms for sperm sorting technologies are being developed to address the shortcomings of conventional centrifugation techniques. To gain a better understanding of natural sperm selection and avoid the complications faced in *in vivo* studies, researchers have simulated the interaction between the female genital tract and the sperm on microfluidic platforms.[10,27–30] These microfluidic platforms are based

[a]*Department of Electrical Engineering and Computer Science, Florida Atlantic University, Boca Raton, FL 33431, USA. E-mail: wasghar@fau.edu*
[b]*Asghar-Lab, Micro and Nanotechnology in Medicine, College of Engineering and Computer Science, Boca Raton, FL 33431, USA*
[c]*Department of Biological Sciences (Courtesy Appointment), Florida Atlantic University, Boca Raton, FL 33431, USA*
†Electronic supplementary information (ESI) available. See DOI: 10.1039/d1an02311j

on hydrostatic pressure, magnetophoresis, optical trap, gravity, or rheotaxis to sort the sperm cells.[28,29,31–35] Multiple rheotaxis-based chips have been developed resulting in improved sperm mortality and normal morphology.[10,27,28,35–43] However, previous microfluidic device designs exhibit several shortcomings, including entrapment of only a few cells for a brief time frame,[28,44] issues in releasing sperm cells if too many enter the channel,[44] requirements of complex equipment for device functioning and simultaneous capture of non-motile and dead sperm cells.[10,35] One of the major limitations of these devices is that they do not allow the collection of sorted sperm cells for further analysis. ESI Table 1† illustrates comparisons of existing microfluidic devices in terms of motility, sperm DNA fragmentation (SDF), morphology analysis, and recovery rate, along with their limitations. Therefore, there is a need to develop microfluidic devices that can improve the sperm selection process allowing easy collection of healthy sperm with better motility, morphology and DNA fragmentation.

To overcome these limitations, our developed microfluidic chip offers a platform where the sperm cells experience different shear stress in different parts of the chip that facilitates the isolation of competent sperm cells without impacting their integrity. Simultaneously, it also allows effortless collection of sorted sperm cells from the collecting chamber, which holds clinical significance. The shear stress inside the device is generated by fluid flow at 0.5 μL min^{-1} flow rate using a syringe pump. A raw semen sample is then added to the sample inlet chamber from where motile sperm cells will swim towards the collecting chamber, effectively separating themselves from dead and immotile sperm. For comparison, we used another chip with no-flow (control) conditions. Sperm cells isolated from the collecting chamber of the with-flow group exhibit significantly higher motility (99 ± 0.62%), a higher number of morphologically normal cells (61.56 ± 1.93%), and substantially lower DNA fragmentation (2.6 ± 1.04%) compared to the stock (unprocessed semen sample) and no-flow (control) sample. The microfluidic chip with-flow has presented overall better results in terms of motility, SDF, morphology analysis and accessible collection of sorted sperm cells compared to our no-flow (control) chip and existing rheotaxis-based microfluidic devices. This microfluidic device selects healthy sperm exhibiting positive rheotaxis while minimizing contamination by deformed or dead sperm cells.

Materials and methods

Device fabrication

We used a silicon wafer for mold fabrication. The layout of the microfluidic chip was designed in AutoCAD software and was printed on a mask film. Using photolithography, the design was transferred onto a silicon wafer using SU8 photoresist (Microchem, Westborough, MA) in the cleanroom at Advanced Materials Engineering Research Institute (AMERI), Florida International University (Miami, USA). The wafer was methodically cleaned, and the negative photoresist SU-8 was spin-coated at 3000 rpm for 30 seconds to achieve the thickness of ~100 μm covering layer followed by soft baking at 65 °C for 10 min and 95 °C for 30 min. The silicon wafer with SU8 resist on it was exposed to i-line at 350 nm to imprint the microfluidic chip pattern on the wafer. The photoresist on the unexposed areas was solidified by hard-baking at 65 °C for 1 min and 95 °C for 10 min. Following the development, the substrate was rinsed with isopropyl alcohol and dried with nitrogen.

To make the device flexible and optically transparent, we used Polydimethylsiloxane (PDMS) for the microfluidic chip preparation bonded onto the glass slide. PDMS elastomer and PDMS curing agent from the Sylgard ® 184 Silicone Elastomer Kit (Dow Corning, Midland, MI, USA) were mixed in a 10 : 1 ratio. The mixture was centrifuged at 1200 rpm for 5 minutes and poured on the immobilized silicon wafer in the Petri dish. The Petri dish containing the PDMS mixture was subjected to vacuum conditions for about 15 minutes to remove all the air bubbles, followed by the overnight baking at 60 °C in the oven. After baking, the chambers on the PDMS were punched using a hole puncher. A 1.5 mm, 6 mm, 4 mm, and 8 mm diameter hole puncher was used for the flow inlet chamber, collecting chamber, sample inlet chamber, and waste collection chamber, respectively. 50 ml of the PDMS mix poured onto the immobilized wafer provides about 3 mm of thickness. The PDMS pieces and glass slides were sonicated separately for 15 minutes in 70% ethanol and dried using nitrogen gas to obtain the clean microfluidic chip. For the bonding of PDMS pieces to the glass slides, both were treated in the oxygen plasma for about 3 minutes using plasma cleaner. The PDMS pieces were attached to glass slides, and the Cole-Parmer Microbore Tubing, 0.050″ × 0.090″ OD was connected to the flow inlet chamber using epoxy glue (Loctite epoxy) which dries within 15 minutes.

Human tubal fluid (HTF) preparation

HTF (FisherSci, Hanover Park, IL) and 1% bovine serum albumin (BSA) (FisherSci, FairLawn, NJ) solution was used to maintain the optimal physiological pH environment for the sperm cells in the microfluidic chip. Before loading the chip with HTF buffer supplemented with 1% BSA, the buffer solution was incubated for 15 minutes at 37 °C in a hot water bath. This buffer solution was filled in 10 ml of syringe (Becton, Dickson and Company, Franklin Lake, NJ) attached to a 17-gauge blunt needle (SAI, Lake Villa, IL). The blunt end of the needle was connected to the tubing, whose other end was linked to the flow inlet chamber on the microfluidic chip. The syringe was then positioned on the syringe pump (New Era Pump Systems, East Farmingdale, NY), and the HTF buffer was pumped into the chip until the chambers were filled.

Semen sample processing

Unprocessed raw semen samples were purchased from California Cryobank, Fairfax, VA, and Cryos International, Orlando, FL. The samples were shipped and stored in liquid

nitrogen. Before use, the semen samples were thawed at 37 °C in the hot water bath for 15 minutes.

Experimental setup

Different flow rates (0.5 μL min^{-1}, 1 μL min^{-1} & 2 μL min^{-1}) were initially used for this investigation. To maintain the human body temperature in this experimental setup, the microfluidic chips were placed on the hot plate at 35 °C, and both sample inlet and collecting chambers were enclosed with scotch tape. For comparison, a control chip with no-flow conditions was used with the same experimental settings. A high flow rate of 10.5 μl min^{-1} was maintained inside the microfluidic channels until the raw semen sample (stock) was introduced into the inlet chamber. For the stock loading, the scotch tape was removed from the sample inlet chamber, and 17 μl of the semen sample was loaded into the chamber and gently closed again with the scotch tape. After the stock loading, the flow rate was reduced to 0.5 μl min^{-1} for the with-flow chip and 0 μl min^{-1} for the no-flow (control) chip. The avg. flow velocity of the with-flow (at 0.5 μl min^{-1}) chip is 43.8 μm s^{-1}. These experimental settings were maintained for 60 minutes. For the sample collecting, channel "b" (Fig. 1) was blocked manually by gently pressing with the forceps, and 70–80 μl of the buffer sample was collected from the collecting chamber. For each parameter assessment, the experiments were repeated at least three times (N = 3), and at least 100 sperm cells (n = 100) were observed from each sample. The results are presented with average and ±standard deviation in the graphs.

COMSOL analysis

The microchannels in microfluidic devices perform a fundamental task that influences dimension, shear stress, and velocity. Therefore, we performed COMSOL simulation on this developed microfluidic chip using COMSOL Multiphysics 4.2

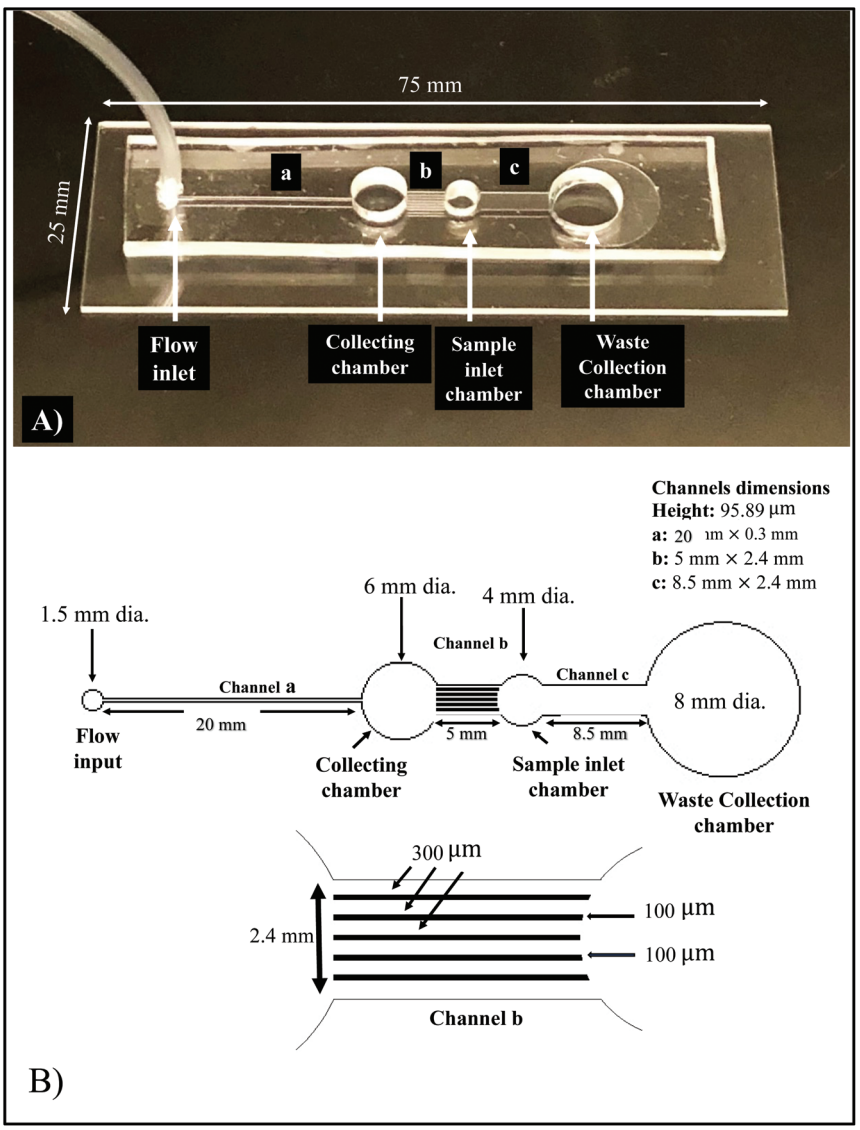

Fig. 1 (A) Image of the assembled PDMS microfluidic chip. (B) Schematic of the microfluidic chip illustrating the detailed layout.

software. Water was used as the sample fluid to simulate log velocity and log shear stress profiles. The laminar flow was calculated, no-slip boundary conditions were applied to the walls of the microfluidic chip, and outlet pressure was assumed to be zero. Navier–Stokes equation was applied with an inlet flow rate of 0.5 μl min^{-1} to solve the simulation with different sizes of meshes. COMSOL results are presented in the ESI.†

Sperm concentration

For the concentration assessment, sperm from the stock, control and with-flow chips, were counted using Makler counter (Sefi Medical, Israel). 1 μl of the sperm sample was analyzed manually according to the manufacturer's instructions. The sperm cells were counted three times for each sample post collection, and the average was used for data points.

Velocity analysis

For velocity evaluation, stock and buffer samples were collected from the chips (no-flow & with-flow), prepared, and examined as per the WHO (World Health Organization Laboratory Manual for the Examination and processing of Human Semen 2010) guidelines.[18] To attain a depth of 20.7 μm, 6.5 μl of the recovered sperm sample was loaded onto a clean glass slide and covered with an 18 × 18 mm coverslip. All the sperm cells were observed using an optical microscope, and the videos were captured using a Nikon DS-Fi3 camera with NIS-Elements software (Nikon) attached to a light microscope. The swimming pattern of each sperm cell from a different location of the glass slide was recorded for 15 seconds at 30 fps to monitor the velocity parameters. The videos were processed in ImageJ (National Institute of Health, http://rsbweb.nih.gov/ij/) using CASA plugin to obtain different velocity parameters, *i.e.*, straight-line velocity (VSL), curvilinear velocity (VCL), and average path velocity (VAP).[10,27,45]

Sperm morphology assessment

The sperm cells from the stock sample as well as sperm cells recovered from the chips with no-flow and with-flow settings were used for the morphology assessment. 2–4 μl of the sperm sample was placed on ready-to-use Millennium Science Cell-VU pre-stained-glass slides (FisherSci, FairLawn, NJ) and covered with a 24 × 24 mm coverslip. Sperm morphology was determined using the WHO strict guidelines as follows: sperm cells should exhibit an oval, smooth, regularly contoured head; contain 40–70% acrosome with no large vacuoles or no more than 2 vacuoles; exhibit a midpiece aligned to the head with the same length as the head and possessing the same regular slender shape in addition to approximately 45 μm long principal piece with no sharp angles. As long as sperm met these criteria, they were considered morphologically normal.[46] At least 100 sperm cells (n = 100, N = 3) were assessed from each sample under the 40× objective using a bright field microscope.

DNA fragmentation

To determine sperm DNA fragmentation (SDF), we used a Halosperm G2 kit (Spectrum Technologies, Inc., CA). An aliquot of stock sample was prepared by diluting 20 million sperm per mL in HTF buffer. No dilution was prepared for the samples recovered from the chips (no-flow and with-flow). The samples were mixed with agarose gel in a 1 : 2 ratio, pipetted onto a pre-coated slide, and covered with a coverslip. The slides were then transferred into the fridge at 4 °C for 5 minutes. After 5 minutes, the coverslips were gently removed, and the slides were immersed horizontally in solution 1 (denaturant agent) for 7 minutes and solution 2 (lysis solution) for 20 minutes. Subsequently, the slides were washed with distilled water for 5 minutes, dehydrated with 70% ethanol and 100% ethanol for 2 minutes each, and air dried. Finally, for the staining, solution 3 (eosine staining solution A) and solution 4 (thiazine staining solution B) were applied sequentially for 8 minutes each. For the analysis, sperm cells were immediately observed using a bright field-microscope under the 40× objective. From each sample, 100 spermatozoa (n = 100, N = 3) were examined.

Statistical analysis

One-way analysis of variance (ANOVA) was performed for the statistical analysis on all the three studied groups (stock, control, and with-flow). A p-value of $\leq$0.05 was considered statistically significant between the groups.

Results

Fig. 1(A) shows the fully assembled PDMS chip. The microfluidic chip consists of 4 cylindrical chambers that are connected through the microchannels. The four chambers are the fluid inlet chamber, collecting chamber, sample inlet chamber, and waste collection chamber (Fig. 1(B) illustrates the detailed layout of the chip). The channel between the fluid inlet and the collecting chamber (labeled as "a") is 0.3 mm wide and 20 mm long. The channel between the collecting chamber and sample inlet (labeled as "b") contains microgrooves to guide the sperm cells in addition to the fluid flow for the rheotaxis movement of the sperm cells towards the collecting chamber. Channel "b" is 5 mm long and 2.4 mm wide and consists of six 300 μm wide microgrooves separated by five 100 μm wide walls. The channel between the sample inlet and waste chamber (labeled as "c") is 8.5 mm long and 2.4 mm wide, which floods non-motile or immature cells towards the waste collection chamber. Photolithography design produced a channel height of 95.89 μm for all channels. Fig. S1† represents the 3D image of the microfluidic chip designed in COMSOL.

With-flow sperm group shows better motility

The motility of the stock, no-flow and with-flow samples were calculated. Graphical representation of motility and isolation efficiency of sperm cells is illustrated in Fig. 2. Unsorted semen sample concentration was greater than 15 million per mL in the experiments and lies anywhere between 96–170 × 10^6 cells per mL. The motility was assessed based on immotile

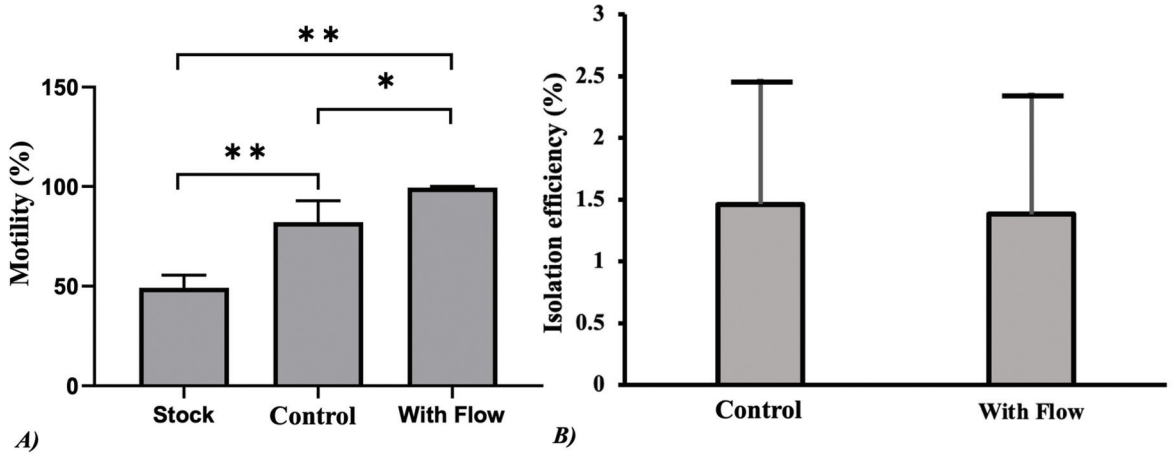

Fig. 2 Comparison of (A) motility and (B) isolation efficiency of sperm cells from three studied groups. The bar on the top represents the statistical significance between the samples (**p-value < 0.01 and *p-value < 0.05).

and motile sperm cells present in the samples. The average motility of the stock sample was approximately 49 ± 6.38%, which was much lower than the experimental control group, holding 81 ± 0.04% and the with-flow group showing 99.47 ± 0.62% (Fig. 2A). The motility % of the chip with-flow conditions was significantly higher than the stock and control group. A one-way ANOVA analysis illustrates that the results of these samples are statically different (**p-value < 0.01 and *p-value < 0.05). Additionally, the isolation efficiency of the motile cells in the sample collected from the control chip shows 1.9×10^5 to 1.6×10^6 sperm per mL (1.46 ± 1%), and with-flow conditions lies anywhere between 1.4×10^5 to 9.9×10^5 sperm per mL (1.38 ± 0.97%) (Fig. 2B).

With-flow group has higher sperm velocity

For the velocity analysis, the videos of multiple sperm cells were recorded. Due to the low concentration of the sperm cells in the samples recovered from the control and with-flow chip, most of the recorded videos contain a single sperm cell for velocity analysis. Based on the swimming pattern and speed of the sperm, the average of the VCL, VAP, and VSL was observed using the CASA plugin. The graph in Fig. 3 represents the velocity parameters of stock, control, and with-flow group. The sperm cells isolated from the with-flow group showed higher VCL and VAP values than stock and control. Conversely, the VSL value of the with-flow group was lower than the stock but higher than the control. The difference in these groups is statistically insignificant. Video S1(A–C)† represents the sperm track used to analyze various velocities from stock, control, and with-flow group.

With-flow group demonstrated a high rate of normal morphology

For the standard sperm morphology assessment, WHO manual guidelines were strictly followed to examine the morphology of the sperm cells from stock and the sample collected from with-flow and no-flow chip settings (Fig. 4). The sperm

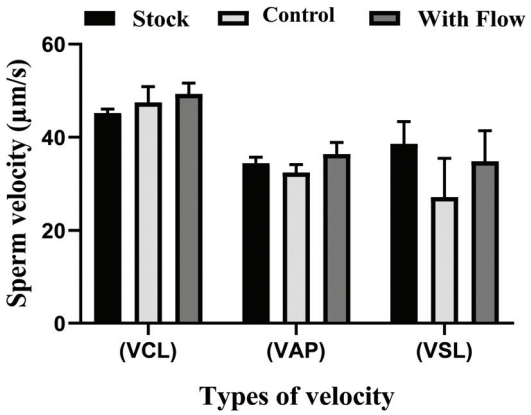

Fig. 3 The graph represents the velocity analysis of sperm cells. Curvilinear velocity (VCL), average path velocity (VAP), and straight-line velocity (VSL) of the three studied groups. (n < 100, N = 3).

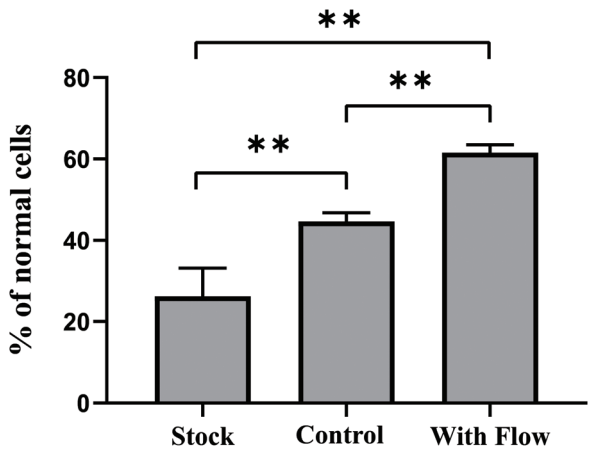

Fig. 4 The percent of morphologically normal sperm cells from three studied groups. The bar on the top represents the statistical significance between the samples (**p-value < 0.01) (n = 100, N = 3).

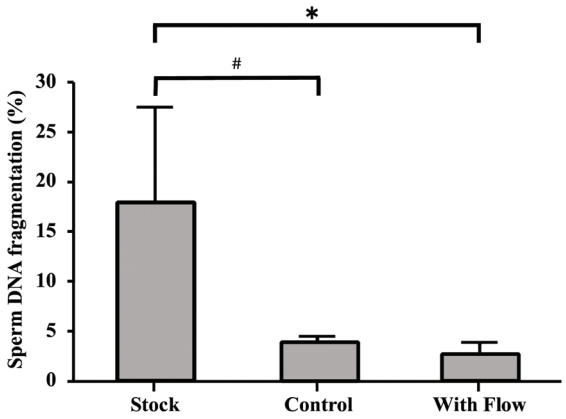

Fig. 5 DNA fragmentation analysis of sperm cells from three studied groups. The bar on the top represents the statistical significance (*p-value = 0.05 for with-flow). No difference for no-flow (control) group (#p-value = 0.06) (n > 100, N = 3).

cells from the with-flow condition hold the highest average morphological normality 61.56 ± 1.93%, in comparison to the stock and the control, showing 26.25 ± 6.91% and 44.65 ± 2.41% respectively. The data was statistically significant (**p < 0.01) between the groups when compared using ANOVA analysis. Fig. S2(A–C)† show 40× objective brightfield images of the sperm cells illustrating the morphology of stock, control, and with-flow sample respectively.

With-flow group exhibited significantly lower SDF

Sperm with a big and medium halo, *i.e.*, similar width as the diameter of the core, are considered non-fragmented. The cells with a small halo, without a halo, or degraded are considered to exhibit fragmented DNA. Sperm cells sorted with the with-flow and control settings show significantly lower SDF% than stock (Fig. 5). The SDF of stock, control, and with-flow are 17.89 ± 9.5%, 3.9 ± 0.33% and 2.6 ± 1.04%, respectively. Improvement in DNA quality was observed with the control (74%) and with-flow (84%) groups. Significant difference in SDF was observed (p = 0.05) between stock and with-flow groups, however, no significant difference (p = 0.06) was observed between the stock and no-flow group. Fig. S3(A–C)† are 40× objective brightfield images of the sperm cells illustrating DNA fragmentation analysis of stock, control, and with-flow samples, respectively.

Discussion

Microfluidic platforms have provided solutions for an extensive range of clinical complications in sperm sorting.[13,41,47] For example, microfluidics have allowed for clean separation of sperm from semen, which is imperative for ART as the zinc and prostaglandins present in semen often hinder fertilization.[48] Additionally, microfluidic sperm sorting devices are advantageous because they can process small amounts of sample, time and cost-efficient, and offer high throughput with better motile sperm retrieval. The chip described in this paper offers all the aforementioned benefits with greater efficiency and less DNA fragmentation compared to other devices in the literature and utilizes rheotaxis as a natural selection mechanism.

In this research, several flow rates were investigated initially for the rheotaxis-based filtration process on the chip. Fig. S4† illustrates the isolation efficiency of sperm cells at different flow rates. The graph shows that 0.5 μL min^{-1} is an optimal flow rate for isolation efficiency compared to 1 μL min^{-1} and 2 μL min^{-1}. Therefore, we selected 0.5 μL min^{-1} for this research to isolate healthy sperm cells. Video S2(A–C)† (captured with 40× objective) illustrates the difficulty faced by sperm cells while entering channel "b" at 2 μL min^{-1}, 1 μL min^{-1} and 0.5 μL min^{-1} flow rates respectively. Sperm cells face high force when the flow rate is 2 μL min^{-1} and 1 μL min^{-1}. However, at 0.5 μL min^{-1} flow rate, the motile cells are smoothly entering the channel "b". These videos show that an optimal fluid flow influences the isolation of motile and morphologically normal sperm cells. To avoid contamination in the collecting chamber, the stock sample was introduced to the sample inlet chamber at a flow rate of 10.5 μl min^{-1}. This high flow rate induced high shear force in channel "b", prohibiting sperm cells from entering the channel "b". Video S3(A)† (captured with 20× objective) shows the behavior of sperm cells when the flow rate is 10.5 μl min^{-1}. Once the flow rate was reduced to 0.5 μl min^{-1}, the sperm cells aligned against the flow and swam towards the collecting chamber. The Video S3(B)† (captured with 20× objective) shows that the sperm cells are actively swimming against the flow (0.5 μL min^{-1}) towards the collecting chamber from the sample inlet chamber. A decrease in the shear force experienced by the cells in channel "b" resulted in swimming against the direction of the flow. Additionally, grooves inside the channel also guided the cells to swim towards the collecting chamber and increase the sperm quantity in the collecting chamber. In the female reproductive tract, 10–20 μm longitudinal microgrooves are entrenched in the bovine cervix, guiding the sperm cells towards the fallopian tubes.[42,43] Therefore, to increase the quantity, grooves inside channel "b" were designed. The flow rate of the mucus in the female reproductive system remains unknown, however, these observations strongly suggest that the fluid flow rate in the oviduct significantly influences sperm cell migration towards the oocyte. Once the sperm cells reach the collecting chamber, they cannot swim further as channel "a" width is reduced. This reduced width generates a high flow that prevents the cells from entering channel "a"; hence the cells are retained in the collecting chamber. Video S4† (captured with 40× objective) is a 10-second video illustrating the hindrance faced by sperm cells due to the high flow rate in channel "a". We also recorded Video S5† when no-flow conditions were maintained in the chip after semen loading. Under the no-flow condition, morphologically abnormal sperm cells along with normal ones can also be seen entering the channel "b" easily. The arrows in the video represent morphologically abnormal cells.

The velocity computation-based model of the microfluidic chip (Fig. S5A†) demonstrated that the sperm cells experience different velocities in different parts of the chip that facilitate the competent sperm filtration process. Additionally, Fig. S5B† simulation shows that channel "b" has higher velocity in the center and lower against the walls. This aligns the sperm head towards the wall, resulting in experiencing less force. This is the cause: only functional and motile sperm cells to swim against the flow and progress towards the collecting chamber. The immature sperm cells and morphologically abnormal cells are retained in the sample inlet chamber. The shear stress profile Fig. S5C† shows that sperm cells in the collecting chamber experience lower stress, therefore, they can be retained in the chamber for a long time without getting exhausted, which can be harmful to their motility. At the same time, shear profile Fig. S5D† shows that the sperm cells in channel "b" do not experience high shear stress in the center, which is why lesser damage to the cell structure was seen. 0.5 μL min^{-1} flow rate in channel "b" offers optimal shear stress conditions that allow the maximum number of sperm cells to swim towards the collecting chamber.

The experimental results from this microfluidic chip have shown 99.47 ± 0.62% motility which is a much better outcome than the previous studies based on rheotaxis (~83%,[10] 32.58%,[35] ~95%,[29] 85%,[27] only ±7% difference between the collected and raw semen sample[44]). Sperm motility is one of the important parameters for the sperm cell that determines fertilization rate. It helps the sperm cell to penetrate the zona pellucida, both *in vivo* and *in vitro*.[49] A significant difference in sperm motility is observed between all three studied groups. The with-flow group demonstrated the highest motility compared to the control and stock. The with-flow chip shows motility closer to 100%. This shows that our chip can be readily implemented for clinical application. The microfluidic chips, with-flow and no-flow conditions, showed a low cell count in the collecting chamber in terms of isolation efficiency. However, it is important to mention here that the with-flow chip contained only motile sperm cells, which is an important factor for successful ART. This microfluidic chip with-flow selects healthy cells which can be used for ICSI processing. Although the cells in the collecting chamber are low in count, the chip offers a pool of competent cells to fertilize the oocyte. ICSI procedure requires only 10–30 healthy sperm cells for successful fertilization.[50] The developed chip provides more than enough cells required for a successful ICSI procedure.

Kinematics of motile sperm cells collected from all the three studied groups (stock, control, and with-flow) were analyzed. The sperm cells collected from the with-flow group showed the higher VLC presenting that sperm can travel a large distance against the flow. In Video S3(B),† it is seen that only the motile cells can swim against the stream from the inlet chamber and the cells with high abnormalities (bent head, broken tail, and immature sperm cells) cannot enter channel "b" due to the flow. This also validates that rheotaxis selects the healthy, motile, and higher velocity sperm cells for the fertilization process.

A higher number of morphologically normal sperm in the sample is correlated with a higher pregnancy rate.[50] For the functional parameters, the morphology of the sperm cells collected from stock, control, and with-flow was examined. A significant difference in sperm morphology was observed between the three groups. The cells obtained from the with-flow group provided the highest percentage of morphologically normal sperm cells, whereas the stock sample contained the lowest percentage of morphologically normal cells. For procedures like ICSI, normal morphology selection is imperative. This rheotaxis-based with-flow chip successfully isolates a large number of morphologically normal sperm cells that can be used for ICSI methods. One study even found that adhering to strict morphology criteria increased fertilization probability from 40% to 97%.[51]

Loosely packed chromatin and a high level of DNA fragmentation abnormalities in sperm nuclei could affect embryo development.[52] The recent shift of the ART technology focuses on the approaches that isolate "healthy" sperm cells, majorly considering sperm DNA integrity as an important factor.[53] If DNA damage is slight in a sperm cell, the oocyte can repair it but, if the damage is high, then the oocyte fails to repair it. High SDF can adversely affect the outcome in the ART cycle.[54,55] We observed that the sperm sorted from the chip with-flow conditions showed significantly lower SDF compared to stock. Sperm cells from an infertile man have a higher rate of SDF compared to those of fertile men.[38,56] The result from this study shows that the chip isolates a significantly higher number of sperm cells with lower SDF, which is a crucial parameter for the fertilization process. The control chip also isolated cells with low SDF, but the difference is statistically insignificant. We used the Halosperm G2 kit for SDF analysis. The kit uses sperm chromatin dispersion technique (SCD).[57] After treatment with solutions 1 and 2, DNA in the cells is denatured, fragmented and nuclear proteins are removed. When there is an absence of significant breakage in sperm DNA, the nucleoids produce a large halo of scattering DNA loops. And nucleoids from fragmented cells do not show any halo.[58]

Overall, the with-flow chip has shown better results than the control group in terms of motility, morphology analysis and DNA fragmentation with significant differences. ICSI requires only one sperm cell to fertilize an oocyte.[59–64] The cells in the collecting chamber of the with-flow group are sufficient in quantity to meet the minimum requirement of ICSI. This chip can be used for ICSI practices since it offers plenty of motile and functional cells with good morphology and high DNA integrity. The current centrifugation methods require multiple steps, multiple types of equipment and take about 2 hours to isolate sperm cells. The operating procedure of the chip is very easy. Once the semen is loaded into the sample inlet chamber, the competent sperm cells start moving against the fluid flow towards the collecting chamber from where they can easily be collected. This chip offers a one-step, one-hour operational benefit which an operator can use with minimal training. The assembly of the microfluidic chip is

low-cost, and the reagents used in the chip to separate sperm cells are only a few milliliters (2–3 mL), therefore, the commercial cost of the chip would be less than $5.00. This will considerably reduce the economic burden of fertility implementations. Taken together, both the chip and the sperm cells isolated from it offer great clinical significance and applicability.

Conclusion

The application of microfluidics in semen analysis can help select normal and functional sperm cells. The developed microfluidic chip does not require a highly skilled technician to operate as the semen loading and sample collection process is straightforward. The utilization of the developed chip demonstrates that the fluid flow in the channel directs the upstream swimming of functional sperm cells towards the collecting chamber while simultaneously washing away the immotile and abnormal cells. Furthermore, microgrooves present in the channel facilitate sperm movement towards the collecting chamber. The results from the chip with-flow demonstrated a high motility percentage and high amount of morphologically normal cells with an 84% improvement in DNA integrity. The amount and quality of sperm cells isolated using the chip are enough for ICSI. Notably, the isolation efficiency of with-flow and no-flow groups was observed to be almost the same, however, the overall results demonstrate that fluid flow isolates higher-quality of motile sperm with low DNA fragmentation and enhanced morphology. Conventional centrifugation often compromises sperm cell integrity, and this study shows that our microfluidic chip eliminates this issue. Our chip is inexpensive, easy to operate, and efficiently isolates healthy sperm, providing seamless integration for clinical application.

Author contributions

W. A. and S. S. designed research and methodology; S. S. developed research design, performed research. S. S. and W. A. analyzed the data and interpreted the results. M. A. K. contributed to the mold fabrication; and W. A. was the principal investigator of the group. All authors contributed to the manuscript writeup.

Conflicts of interest

The authors declares that they have no conflict of interest.

Acknowledgements

We would like to thank Amy Makler and Kristina Fritz for reviewing the manuscript and providing valuable comments and suggestions. We also acknowledge support from College of Engineering and Computer Science, Florida Atlantic University, Boca Raton, FL.

References

1 Z. Zhang, J. Liu, J. Meriano, C. Ru, S. Xie, J. Luo and Y. Sun, *Sci. Rep.*, 2016, **6**, 1–8.
2 D. Fordney-Settlage, *Int. J. Fertil.*, 1981, **26**, 161–169.
3 D. A. Vaughan and D. Sakkas, *Biol. Reprod.*, 2019, **101**, 1076–1082.
4 K. Miki and D. E. Clapham, *Curr. Biol.*, 2013, **23**, 443–452.
5 H. Shafiee, W. Asghar, F. Inci, M. Yuksekkaya, M. Jahangir, M. H. Zhang, N. G. Durmus, U. A. Gurkan, D. R. Kuritzkes and U. Demirci, *Sci. Rep.*, 2015, **5**, 8719.
6 S. Pérez-Cerezales, S. Boryshpolets, O. Afanzar, A. Brandis, R. Nevo, V. Kiss and M. Eisenbach, *Sci. Rep.*, 2015, **5**, 1–18.
7 S. Pérez-Cerezales, S. Boryshpolets and M. Eisenbach, *Asian J. Androl.*, 2015, **17**, 628.
8 D. Ralt, M. Manor, A. Cohen-Dayag, I. Tur-Kaspa, I. Ben-Shlomo, A. Makler, I. Yuli, J. Dor, S. Blumberg and S. Mashiach, *Biol. Reprod.*, 1994, **50**, 774–785.
9 A. Bahat and M. Eisenbach, *Mol. Cell. Endocrinol.*, 2006, **252**, 115–119.
10 K. Rappa, J. Samargia, M. Sher, J. S. Pino, H. F. Rodriguez and W. Asghar, *Microfluid. Nanofluid.*, 2018, **22**, 1–11.
11 T. El-sherry, M. Abdel-Ghani, N. Abou-Khalil, M. Elsayed and M. Abdelgawad, *Reprod. Domest. Anim.*, 2017, **52**, 781–790.
12 Y. Ishikawa, T. Usui, M. Yamashita, Y. Kanemori and T. Baba, *Biol. Reprod.*, 2016, **94**(89), 81–89.
13 T. Chinnasamy, J. L. Kingsley, F. Inci, P. J. Turek, M. P. Rosen, B. Behr, E. Tüzel and U. Demirci, *Adv. Sci.*, 2018, **5**, 1700531.
14 X. Zhang, I. Khimji, U. A. Gurkan, H. Safaee, P. N. Catalano, H. O. Keles, E. Kayaalp and U. Demirci, *Lab Chip*, 2011, **11**, 2535–2540.
15 G. Griesinger, C. Blockeel, P. Pierzynski, H. Tournaye, H. Višňová, A. Humberstone, P. Terrill, O. Pohl, E. Garner and J. Donnez, *Hum. Reprod.*, 2021, **36**, 1007–1020.
16 B. Luke, M. B. Brown, E. Wantman, A. Lederman, W. Gibbons, G. L. Schattman, R. A. Lobo, R. E. Leach and J. E. Stern, *N. Engl. J. Med.*, 2012, **366**, 2483–2491.
17 D. Liu and H. Baker, *Hum. Reprod.*, 1994, **9**, 489–496.
18 WHO, WHO laboratory manual for the examination and processing of human semenWHO laboratory manual for the examination and processing of human semen, https://www.who.int/publications/i/item/9789240030787, (accessed 28 September, 2021).
19 L. Larsen, T. Scheike, T. K. Jensen, J. P. Bonde, E. Ernst, N. H. Hjollund, Y. Zhou, N. E. Skakkebæk, A. Giwercman and D. F. P. P. S. Team, *Hum. Reprod.*, 2000, **15**, 1562–1567.
20 M. J. Zinaman, C. C. Brown, S. G. SELEVAN and E. D. CLEGG, *J. Androl.*, 2000, **21**, 145–153.
21 D. Liu and H. Baker, *Hum. Reprod.*, 2000, **15**, 702–708.

22 D. Ren, B. Navarro, G. Perez, A. C. Jackson, S. Hsu, Q. Shi, J. L. Tilly and D. E. Clapham, *Nature*, 2001, **413**, 603–609.
23 L. Rienzi, F. Ubaldi, R. Anniballo, G. Cerulo and E. Greco, *Hum. Reprod.*, 1998, **13**, 1014–1019.
24 S. C. Esteves, M. Roque, G. Bedoschi, T. Haahr and P. Humaidan, *Nat. Rev. Urol.*, 2018, **15**, 535–562.
25 Y. Wang, J. Riordon, T. Kong, Y. Xu, B. Nguyen, J. Zhong, J. B. You, A. Lagunov, T. G. Hannam and K. Jarvi, *Adv. Sci.*, 2019, **6**, 1900712.
26 K. L. Rappa, H. F. Rodriguez, G. C. Hakkarainen, R. M. Anchan, G. L. Mutter and W. Asghar, *Biotechnol. Adv.*, 2016, **34**, 578–587.
27 W. Asghar, V. Velasco, J. L. Kingsley, M. S. Shoukat, H. Shafiee, R. M. Anchan, G. L. Mutter, E. Tüzel and U. Demirci, *Adv. Healthcare Mater.*, 2014, **3**, 1671–1679.
28 M. Zaferani, S. H. Cheong and A. Abbaspourrad, *Proc. Natl. Acad. Sci. U. S. A.*, 2018, **115**, 8272–8277.
29 S. Tasoglu, H. Safaee, X. Zhang, J. L. Kingsley, P. N. Catalano, U. A. Gurkan, A. Nureddin, E. Kayaalp, R. M. Anchan and R. L. Maas, *Small*, 2013, **9**, 3374–3384.
30 R. Nosrati, M. Vollmer, L. Eamer, M. C. San Gabriel, K. Zeidan, A. Zini and D. Sinton, *Lab Chip*, 2014, **14**, 1142–1150.
31 D.-B. Seo, Y. Agca, Z. Feng and J. K. Critser, *Microfluid. Nanofluid.*, 2007, **3**, 561–570.
32 Y.-J. Ko, J.-H. Maeng, B.-C. Lee, S. Lee, S. Y. Hwang and Y. Ahn, *Anal. Sci.*, 2012, **28**, 27–27.
33 N. Modak, A. Datta and R. Ganguly, *Microfluid. Nanofluid.*, 2009, **6**, 647–660.
34 L. M. Devenica, B. Grimm, T.-A. Hultum and A. R. Carter, *Optical Trapping and Optical Micromanipulation XIV*, 2017, 103472V.
35 H. Kang, T. An, D. Lee and B. Kim, *Rev. Sci. Instrum.*, 2019, **90**, 084101.
36 I. R. Sarbandi, A. Lesani, M.-M. Zand and R. Nosrati, *Sci. Rep.*, 2021, **11**, 1–8.
37 Y. Yan, H. Liu, B. Zhang and R. Liu, *Micromachines*, 2020, **11**, 793.
38 A. Ataei, A. Lau and W. Asghar, *Microfluid. Nanofluid.*, 2021, **25**, 1–10.
39 V. Kantsler, J. Dunkel, M. Blayney and R. E. Goldstein, *eLife*, 2014, **3**, e02403.
40 B. Zhang, T. Yin and J. Yang, *Anal. Methods*, 2015, **7**, 5981–5988.
41 C.-K. Tung, F. Ardon, A. G. Fiore, S. S. Suarez and M. Wu, *Lab Chip*, 2014, **14**, 1348–1356.
42 C.-K. Tung, L. Hu, A. G. Fiore, F. Ardon, D. G. Hickman, R. O. Gilbert, S. S. Suarez and M. Wu, *Proc. Natl. Acad. Sci. U. S. A.*, 2015, **112**, 5431–5436.
43 M. Zaferani, G. D. Palermo and A. Abbaspourrad, *Sci. Adv.*, 2019, **5**, eaav2111.
44 R. Samuel, N. Miller, O. Badamjav, T. Jenkins, D. Carrell, J. Hotaling and B. K. Gale, *J. Micromech. Microeng.*, 2018, **28**, 097002.
45 C. Alquézar-Baeta, S. Gimeno-Martos, S. Miguel-Jiménez, P. Santolaria, J. Yániz, I. Palacín, A. Casao, J. Á. Cebrián-Pérez, T. Muiño-Blanco and R. Pérez-Pé, *PLoS Comput. Biol.*, 2019, **15**, e1006691.
46 W. Ford, *Asian J. Androl.*, 2010, **12**, 59.
47 M. Simchi, J. Riordon, J. B. You, Y. Wang, S. Xiao, A. Lagunov, T. Hannam, K. Jarvi, R. Nosrati and D. Sinton, *Lab Chip*, 2021, **21**, 2464–2475.
48 C. M. Boomsma, M. J. Heineman, B. J. Cohlen and C. M. Farquhar, *Cochrane Database Syst. Rev.*, 2004, 1465–1858.
49 L. Simon and S. E. Lewis, *Syst. Biol. Reprod. Med.*, 2011, **57**, 133–138.
50 W. Eggert-Kruse, H. Schwarz, G. Rohr, T. Demirakca, W. Tilgen and B. Runnebaum, *Hum. Reprod.*, 1996, **11**, 139–146.
51 A. I. Vawda, J. Gunby and E. V. Younglai, *Hum. Reprod.*, 1996, **11**, 1445–1450.
52 I. Virant-Klun, T. Tomazevic and H. Meden-Vrtovec, *J. Assisted Reprod. Genet.*, 2002, **19**, 319–328.
53 N. Tarozzi, M. Nadalini and A. Borini, in *Genetic Damage in Human Spermatozoa*, Springer, 2019, pp. 169–187.
54 J. H. Martin, R. J. Aitken, E. G. Bromfield and B. Nixon, *Hum. Reprod. Update*, 2019, **25**, 180–201.
55 A. Agarwal and S. Allamaneni, *Minerva Ginecol.*, 2004, **56**, 235–245.
56 L. Simon, I. Proutski, M. Stevenson, D. Jennings, J. McManus, D. Lutton and S. Lewis, *Reprod. BioMed. Online*, 2013, **26**, 68–78.
57 J. L. Fernández, L. Muriel, V. Goyanes, E. Segrelles, J. Gosálvez, M. Enciso, M. LaFromboise and C. De Jonge, *Fertil. Steril.*, 2005, **84**, 860.
58 S. Cankut, T. Dinc, M. Cincik, G. Ozturk and B. Selam, *Reprod. Sci.*, 2019, **26**, 1575–1581.
59 C. C. Ding and K. J. Thong, *Asian J. Androl.*, 2010, **12**, 284.
60 Q. V. Neri, B. Lee, Z. Rosenwaks, K. Machaca and G. D. Palermo, *Cell Calcium*, 2014, **55**, 24–37.
61 S. Xiao, J. Riordon, M. Simchi, A. Lagunov, T. Hannam, K. Jarvi, R. Nosrati and D. Sinton, *Lab Chip*, 2021, **21**, 775–783.
62 A Ataei, M.-A. Kabir, A.-W.-C. Lau and W. Asghar, *F&S Science*, 2021, 376–382.
63 S. Sharma, R. Zhuang, M. Long, M. Pavlovic, Y. Kang, A. Ilyas and W. Asghar, *Biotechnol. Adv.*, 2018, 1063–1078.
64 M.-A. Kabir, R.-S. Acosta, S. Sharma, S.-S. Bradrick, M.-A.-G. Blanco, M. Caputi and W. Asghar, *Sci. Rep.*, 2020, **10**, 11906.